

# Intramolecular Hydrogen Shift Chemistry of Hydroperoxy-Substituted Peroxy Radicals

## Supporting Information

*Eric Praske<sup>a</sup>, Rasmus V. Otkjær<sup>b</sup>, John D. Crounse<sup>c</sup>, J. Caleb Hethcox<sup>a</sup>, Brian M. Stoltz<sup>a</sup>, Henrik*

*G. Kjaergaard<sup>b\*</sup>, Paul O. Wennberg<sup>c,d\*</sup>*

<sup>a</sup> Division of Chemistry and Chemical Engineering, California Institute of Technology, 1200 E.  
California Blvd, Pasadena, CA 91125

<sup>b</sup> Department of Chemistry, University of Copenhagen, Universitetsparken 5, DK-2100  
Copenhagen Ø, Denmark

<sup>c</sup> Division of Geological and Planetary Sciences, California Institute of Technology, 1200 E.  
California Blvd, Pasadena, CA 91125

<sup>d</sup> Division of Engineering and Applied Science, California Institute of Technology, 1200 E.  
California Blvd, Pasadena, CA 91125

\*Correspondence to: Paul O. Wennberg (wennberg@caltech.edu) and Henrik G. Kjaergaard  
(hgk@chem.ku.dk)

## Contents

Experimental .....	3
Synthesis .....	3
RO <sub>2</sub> lifetime calculation.....	5
Calculation of BR <sub>RONO<sub>2</sub></sub> .....	6
Instrumental calibration .....	8
Chromatography .....	10
Uncertainty.....	12
Best fits .....	14
Rapid H-shifts .....	15
Computational.....	17
Tunneling .....	17
OH-Initiated Oxidation of 2-hydroperoxy-2-methylpentane.....	18
OH-Initiated Oxidation of 2-hydroperoxypentane.....	23
Temperature Dependencies.....	26
Values used in the MC-TST equation at 298.15 K.....	28
Values used for the Eckart Tunneling Correction.....	30
Rate Constants at the ωB97X-D/aug-cc-pVTZ level of theory at 298.15 K .....	31
References.....	33

## Experimental

We study the oxidation mechanism of 2-hydroperoxy-2-methylpentane. The reader is referred to the main article for an overview of the method.

### Synthesis

2-hydroperoxy-2-methylpentane is synthesized and purified as described in the main article. The compound is characterized by NMR (see Figure S1) and HR-ToF:  $^1\text{H}$  NMR (400 MHz,  $\text{CDCl}_3$ )  $\delta$  7.27 (br s, 1 H), 1.48-1.44 (m, 2 H), 1.33-1.23 (m, 2 H), 1.15 (s, 6 H), 0.86 (t,  $J = 7.5$  Hz, 1H);  $^{13}\text{C}$  NMR (100 MHz,  $\text{CDCl}_3$ )  $\delta$  82.9, 40.8, 23.8 (2C), 17.3, 14.7; IR (NaCl, film) 3382, 2934, 2872, 2355, 2339, 1455, 1363, 1235, 1175  $\text{cm}^{-1}$ ; HRMS (CI)  $m/z$  203.0898 [ $\text{C}_7\text{F}_3\text{H}_{14}\text{O}_3$  ( $\text{M}+\text{CF}_3\text{O}^-$ ) requires 203.0895].

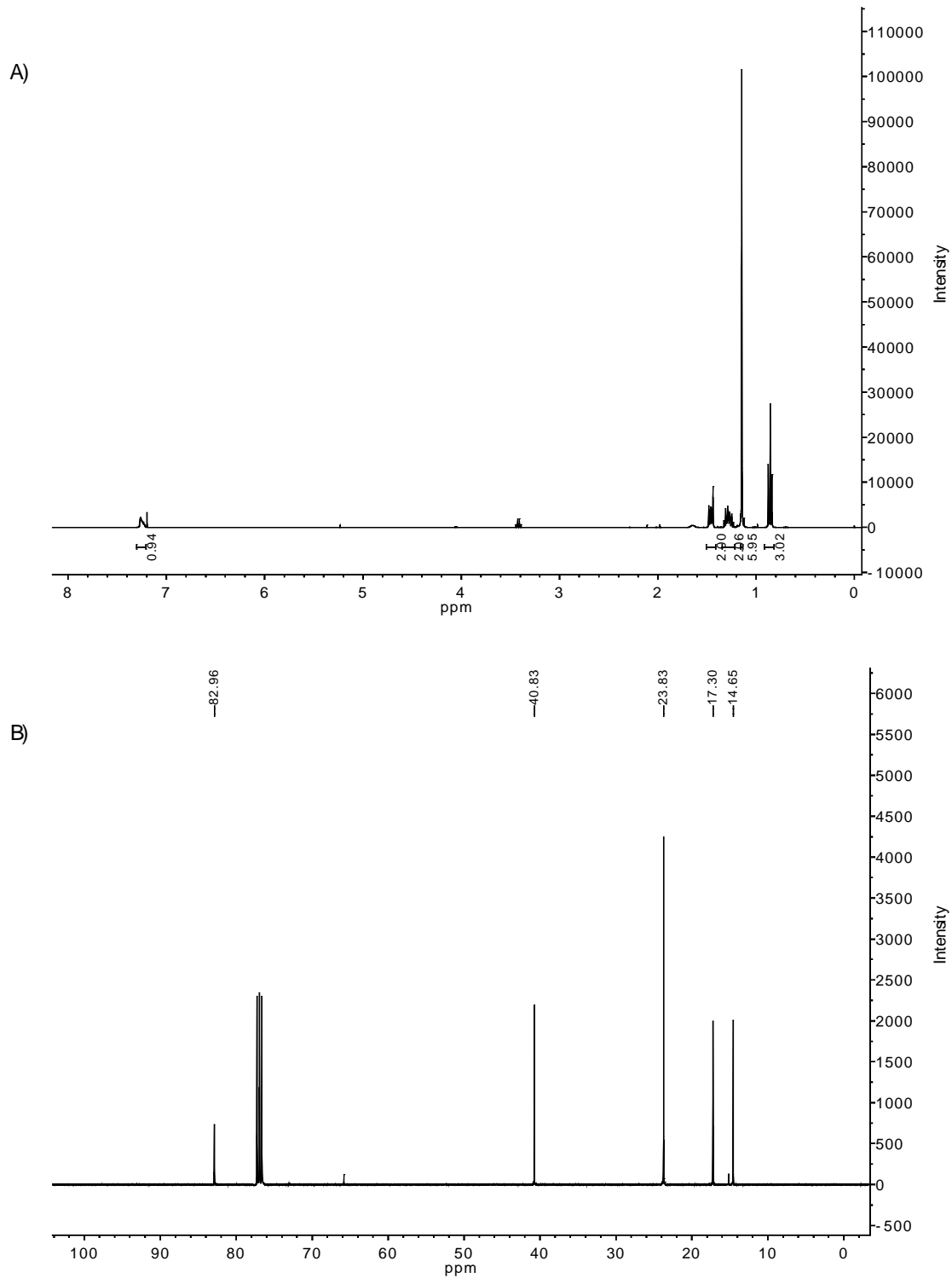


Figure S1. NMR spectra of 2-hydroperoxy-2-methylpentane: A)  $^1\text{H}$  NMR (400 MHz,  $\text{CDCl}_3$ ); B)  $^{13}\text{C}$  NMR (100 MHz,  $\text{CDCl}_3$ )

## RO<sub>2</sub> lifetime calculation

The concentrations of NO and HO<sub>2</sub> are systematically varied, thus producing a range of  $\tau_{\text{bimolecular}}$ . For experiments in which reaction with NO dominates the RO<sub>2</sub> fate,  $\tau_{\text{bimolecular}}$  is calculated based on [NO] measurement. For the remainder,  $\tau_{\text{bimolecular}}$  is calculated as described in Teng et al. and Praske et al.<sup>1-2</sup> This method incorporates an estimate of [NO], building upon the method for estimating [HO<sub>2</sub>] originally described by Crounse et al.<sup>3</sup> Observed production rates of H<sub>2</sub>O<sub>2</sub> ( $P_{\text{H}_2\text{O}_2}$ ), the dihydroperoxide ( $P_{\text{ROOH}}$ ), and hydroperoxy-substituted RONO<sub>2</sub> ( $P_{\text{RONO}_2}$ ) are used to constrain [HO<sub>2</sub>] and [NO]. This is achieved by using recommended values for  $k_{\text{RO}_2+\text{NO}}$ ,  $k_{\text{RO}_2+\text{HO}_2}$ , and  $k_{\text{HO}_2+\text{HO}_2}$ .<sup>4-5</sup> The mixing ratio of HO<sub>2</sub> is given by:

$$P_{\text{H}_2\text{O}_2} = k_{\text{HO}_2+\text{HO}_2} \times [\text{HO}_2]^2$$

$$k_{\text{HO}_2+\text{HO}_2} = \left( 2.2 \times 10^{-13} \exp\left(\frac{600}{T}\right) + 1.9 \times 10^{-33} [\text{M}] \exp\left(\frac{980}{T}\right) \right) \\ \times \left( 1 + 1.4 \times 10^{-21} [\text{H}_2\text{O}] \exp\left(\frac{2200}{T}\right) \right)$$

$$[\text{HO}_2] = \sqrt{\frac{P_{\text{H}_2\text{O}_2}}{k_{\text{HO}_2+\text{HO}_2}}}$$

Using [HO<sub>2</sub>] and the relative yields of ROOH and RONO<sub>2</sub> as input, [NO] can be approximated according to the following equations:

$$P_{\text{RONO}_2} = \text{BR}_{\text{RONO}_2} \times k_{\text{RO}_2+\text{NO}} \times [\text{NO}] \times [\text{RO}_2]$$

$$P_{\text{ROOH}} = \text{BR}_{\text{ROOH}} \times k_{\text{RO}_2+\text{HO}_2} \times [\text{HO}_2] \times [\text{RO}_2]$$

$$[\text{NO}] = \frac{P_{\text{RONO}_2}}{P_{\text{ROOH}}} \frac{\text{BR}_{\text{ROOH}}}{\text{BR}_{\text{RONO}_2}} \frac{k_{\text{RO}_2+\text{HO}_2}}{k_{\text{RO}_2+\text{NO}}} [\text{HO}_2]$$

The branching ratio in the reaction of  $\text{RO}_2+\text{HO}_2$  to yield the hydroperoxide ( $\text{BR}_{\text{ROOH}}$ ) is assumed to be unity and  $\text{BR}_{\text{RONO}_2}$  is calculated as described below.

#### Calculation of $\text{BR}_{\text{RONO}_2}$

The branching ratio of the HPN resulting from reaction of NO with the hydroperoxy  $\text{RO}_2$  cannot be derived in a robust manner using the data. This is due to uncertainty related to the abstraction of the hydroperoxy hydrogen ( $\text{ROO-H}$ ), which likely constitutes a significant reaction channel in the oxidation of 2-hydroperoxy-2-methylpentane by OH. Thus, we use the parameterization of Teng et al. to calculate the branching ratio to form HPN,<sup>6</sup> with corrections applied for  $\beta$ -hydroperoxy and tertiary  $\text{RO}_2$  consistent with the recommendations of Wennberg et al.<sup>5</sup> Accordingly,  $\text{BR}_{\text{RONO}_2}$  is given by:

$$\text{BR}_{\text{RONO}_2} = (0.045 \pm 0.016) \times N - (0.11 \pm 0.05)$$

Where N is the number of heavy atoms excluding the peroxy moiety. For the hydroperoxy-substituted  $\text{RO}_2$ , there are 10 heavy atoms ( $N = 10 - 2 = 8$ ) and the nominal  $\text{BR}_{\text{RONO}_2} = 0.25 \pm 0.08$  at 296 K ( $0.19 \pm 0.06$  at 318 K). The BR for the 2,3  $\text{RO}_2$  is decreased by 60% relative to the nominal  $\text{BR}_{\text{RONO}_2}$ , while the BR for the tertiary  $\text{RO}_2$  is increased by 25%. We use the temperature

dependence determined by Atkinson et al. for the organonitrate yield in the oxidation of n-heptane.<sup>7</sup>

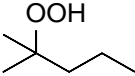
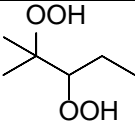
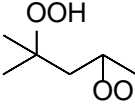
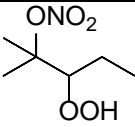
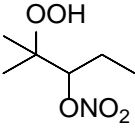
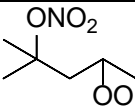
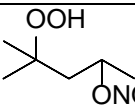
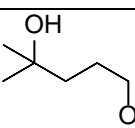
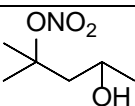
## Instrumental calibration

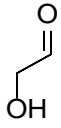
Authentic standards for the multifunctional species presented in this work are not commercially available, thereby precluding a direct calibration for these species. The method of Garden et al. is used for the estimation of instrumental sensitivities.<sup>8</sup> This method employs the parameterization of Su et al. to calculate the ion-molecule collision rate coefficients assuming that all collisions lead to quantifiable product ions.<sup>9</sup> The dipole moments and polarizabilities of closed-shell products are calculated using density functional theory (B3LYP/6-31+G(d)). Due to the dependence of the dipole moment on structural conformation, we use a weighted average of the located conformers. In contrast, the polarizability does not exhibit a large conformational dependence and the determination is based on the lowest energy conformer. These properties for species derived from the 2-hydroperoxy-2-methylpentane system are given in Table S1.

As our estimation of [NO] uses a ratio of production rates ( $\frac{P_{\text{RONO}_2}}{P_{\text{ROOH}}}$ ), the ratio of the calibration factors is also required. The ratio used is an average of the factors for the 2,3 and 2,4 HPN and the 2,3 and 2,4 ROOH. As discussed above, the production rate of H<sub>2</sub>O<sub>2</sub> is used to estimate [HO<sub>2</sub>] and thereby  $\tau_{\text{bimolecular}}$ . The efficiency of CF<sub>3</sub>O<sup>•</sup> clustering with H<sub>2</sub>O<sub>2</sub> is affected by water vapor, and the method described by Praske et al. was adopted to account for this effect.<sup>2</sup> In general, the growth rate of water vapor in our chamber experiments was significantly slower than those reported in Praske et al. due to the use of a dry air purge inside the chamber enclosure. Thus, the corrections for water vapor that were applied resulted in only minimal changes to [HO<sub>2</sub>].



Table S1. Calculated average dipole moments ( $\bar{\mu}$ ) and polarizabilities ( $\alpha$ ) used to determine ion-molecule collision rate coefficients and instrumental sensitivity.  $k_x$  is the conformer weighted average collision rate coefficient. The instrumental sensitivity is derived from the ratio of this rate coefficient for each analyte against that of glycolaldehyde ( $k = 2.0 \times 10^{-9} \text{ cm}^3 \text{ molecule}^{-1} \text{ s}^{-1}$ ), for which an experimental determination has been made. Dipole moments and polarizabilities are calculated at the B3LYP/6-31+G(d) level of theory.

Molecule	$m/z$	$\bar{\mu}$ (D)	$\alpha$ ( $\text{\AA}^3$ )	$k_x$ ( $10^{-9} \text{ cm}^3 \text{ molecule}^{-1} \text{ s}^{-1}$ )	calculated sensitivity ( $\times 10^{-4}$ ) <sup>a</sup>	experimental sensitivity ( $\times 10^{-4}$ ) <sup>a</sup>
	203	1.8	12	1.7	1.8	-
	235	2.6	14	2.1	2.2	-
	235	3.9	14	2.8	2.9	-
	264	4.1	15	2.9	3.0	-
	264	4.2	15	2.9	3.0	-
	264	4.5	15	3.1	3.3	-
	264	4.6	15	3.1	3.3	-
	248	4.3	15	3.0	3.2	-
	248	4.3	15	3.0	3.2	-

Molecule	$m/z$	$\bar{\mu}$ (D)	$\alpha$ ( $\text{\AA}^3$ )	$k_x$ ( $10^{-9} \text{ cm}^3 \text{ molecule}^{-1} \text{ s}^{-1}$ )	calculated sensitivity ( $\times 10^{-4}$ ) <sup>a</sup>	experimental sensitivity ( $\times 10^{-4}$ ) <sup>a</sup>
	145	2.3	4.5	2.0	-	2.1 <sup>b</sup>

<sup>a</sup>  $\text{CF}_3\text{O}^-$  CIMS sensitivity (norm. cts.  $\text{pptv}^{-1}$ )

<sup>b</sup> This value is based on a recent calibration for glycolaldehyde and differs from that reported in Praske et al.<sup>2</sup> Multiple calibrations for various species demonstrated similar increases in sensitivity presumably due to slight differences in the instrumental configuration.

## Chromatography

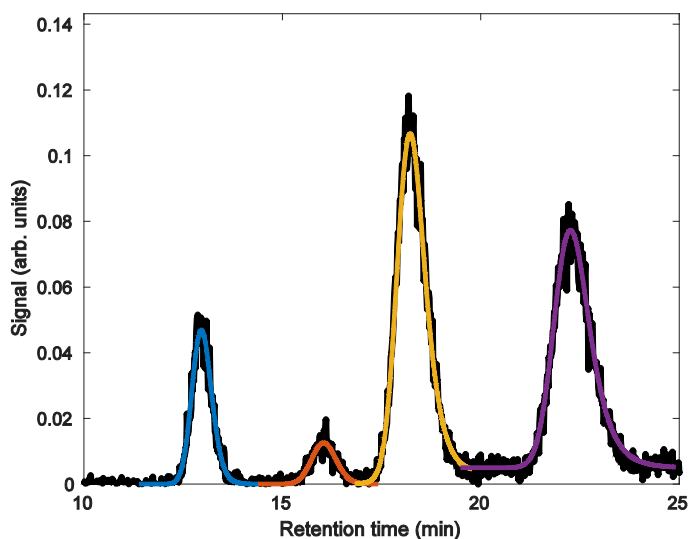


Figure S2. An example chromatogram (black line) for the hydroperoxy-substituted  $\text{RONO}_2$  ( $m/z$  264; neutral mass 179 amu) outlined in Scheme 2, showing the output of the peak fitting algorithm (colored Gaussians). The final two peaks use linear baseline subtraction. See Figure 1 of the main article for assignment.

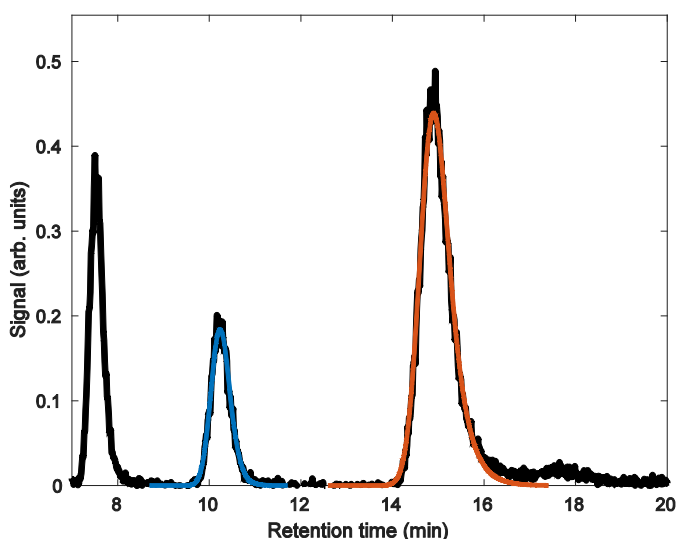


Figure S3. An example chromatogram (black line) for the hydroxy-substituted  $\text{RONO}_2$  ( $m/z$  248; neutral mass 163 amu) outlined in Scheme 3, showing the output of the peak fitting algorithm (colored Gaussians). See Figure 1 of the main article for assignment.

Following oxidation, the  $\text{RONO}_2$  are separated by gas chromatography using a Restek RTX-200 11.5 m column with a column flow of 8 sccm  $\text{N}_2$ . Cryogenic trapping of the analytes is enabled by submersion of a ~20 cm loop of column in an isopropanol bath maintained at  $-20\text{ }^\circ\text{C}$ . It is not possible to significantly lower this temperature without also trapping water, which degrades the chromatography. Upon collection of the sample, the trap is removed and the temperature program is initiated ( $30\text{ }^\circ\text{C}$  for 0.1 min,  $+20\text{ }^\circ\text{C}/\text{min}$  until  $80\text{ }^\circ\text{C}$ , hold at  $80\text{ }^\circ\text{C}$  for 25 min, then  $+20\text{ }^\circ\text{C}/\text{min}$  until  $130\text{ }^\circ\text{C}$ ). The  $80\text{ }^\circ\text{C}$  isothermal elution is necessary to adequately separate the  $\text{RONO}_2$  while minimizing decomposition. The effluent of the column is diluted with  $\text{N}_2$  before being transmitted into the CIMS ion-molecule reaction region. Blank chromatograms are collected prior to the initiation of photooxidation.

Adequate separation of the  $\text{RONO}_2$  is achieved and peak fitting is performed by using an Exponentially Modified Gaussian (EMG) function adapted from MATLAB code by Dr. Tom O'Haver.<sup>10</sup> The peak parameters are fixed and do not vary between experimental runs. A sample

output of the fitting algorithm is shown in Figure S2 and Figure S3. The later eluting isomers exhibit longer tailing and the EMG time constant is adjusted accordingly. All parameters are chosen by minimizing the residuals between the EMG function and the data.

## Uncertainty

Experimental uncertainty can be divided into three main categories: estimation of  $\tau_{\text{bimolecular}}$ , instrument calibration factors, and chromatography. The uncertainty is characterized in a manner similar to that described in Praske et al. and only a brief description is given here.<sup>2</sup> In accordance with the method used to calculate  $\tau_{\text{bimolecular}}$ , we use the observed production rates of hydroperoxides and organonitrates. Linear least-squares fits are used to derive the production rates and we include the  $1\sigma$  error in the slope. Recommended rate coefficients are also used in the estimation of  $\tau_{\text{bimolecular}}$  and these carry associated uncertainty.<sup>4, 11</sup> Finally, calibration factors are assigned a default uncertainty of  $\pm 30\%$ .

Table S2. Bootstrap results expressed as % uncertainty of measured RONO<sub>2</sub> isomer ratios resulting from the peak fits.

	2,4 RONO <sub>2</sub> :2,3 RONO <sub>2</sub>	4-hydroxy-2-methyl-2-nitrooxy:2-hydroxy-2-methyl-5-nitrooxy
$\tau_{\text{bimolecular}} < 20 \text{ s}$	5.0	1.5
$\tau_{\text{bimolecular}} > 20 \text{ s}$	8.5	3.2

The chromatographic uncertainty in the peak fitting algorithm is summarized in Table S2. These values are determined according to a bootstrap method. Two chromatograms are selected for the bootstrap; one is representative of the large signal commonly observed in short lifetime experiments ( $\tau_{\text{bimolecular}} < 20 \text{ s}$ ) and another is representative of the small signal observed in

long lifetime experiments ( $\tau_{\text{bimolecular}} > 20$  s). The bootstrap varies the default peak shape parameters (e.g. in Figure S2) by  $\pm 40\%$  over 10,000 fitting trials. The peak width and tailing factors are expected to be correlated and thus, these parameters are co-varied in the trials. The  $1\sigma$  error of the resulting peak area ratios is expressed in Table S2.

The data points displayed in Figure 3 and Figure 4 carry the aforementioned chromatographic uncertainty as well as uncertainty in  $\tau_{\text{bimolecular}}$ . The best fit, used to derive the experimental rate coefficients in Table 3, is determined by a weighted least squares fit to the data (see Figure S4-S5). The sum of squares is given by:

$$\sum_{i=1}^n \frac{1}{\sigma_i^2} (y_i - \hat{y}_i)^2$$

Where  $\sigma_i^2$  represents the point-wise variance and  $y_i - \hat{y}_i$  denotes the residual between the data points and the model. In order to characterize uncertainty in the experimental factors, a Monte Carlo simulation is conducted. 5,000 synthetic data sets are generated by varying the data points within their respective range of uncertainty and the least squares approach is again adopted to determine the best fit in each of these data sets. The error bounds given in Table 3 represent the full range of values that afforded best fits in the synthetic data sets.

## Best fits

The kinetic model, which employed the calculated rate coefficients in Figure 3 and Figure 4, was used to determine the best fit to the experimental data using the weighted least squares procedure described in previous section. The results that afforded best fits are shown in Figure S4 and Figure S5.

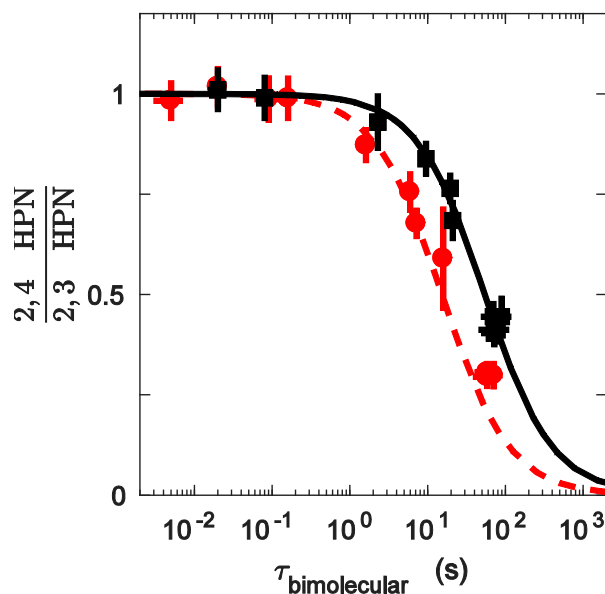


Figure S4. Experimental data used to constrain the  $\alpha$ -OOH 1,5 H-shift at 296 K (black squares) and 318 K (red circles). Best fits are shown at 296 K (solid black line) and 318 K (dashed red line). These fits were used to determine the experimental rate coefficients displayed in Table 3.

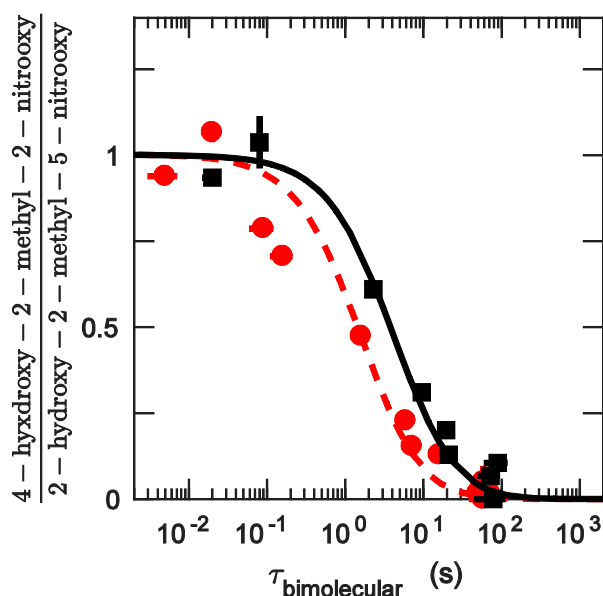


Figure S5. Experimental data used to constrain the  $\alpha$ -OH 1,5 H-shift at 296 K (black squares) and 318 K (red circles). Best fits are shown at 296 K (solid black line) and 318 K (dashed red line). These fits were used to determine the experimental rate coefficients displayed in Table 3.

### Rapid H-shifts

An experimental constraint on the forward rate coefficients ( $k_f$ ) of the rapid H-shifts of hydroperoxy hydrogens (ROO-H) is provided by experimental data collected at very short lifetimes at 296 K. These data are displayed in Figure S6 for the 2,3 RO<sub>2</sub>. For the 2,4 RO<sub>2</sub>, we were unable to demonstrate a decline in the 2-methyl-2-peroxy-4-hydroperoxy isomer and therefore only provide a lower bound estimate of  $k_f > 10^4 \text{ s}^{-1}$ .

A chromatogram collected after oxidation at very short lifetimes is shown in Figure S7. This chromatogram provides further confidence in our assignment of nitrates, as the tertiary nitrate of the 2,3 HPN, and secondary nitrate of the 2,3 HN, disappear. While the tertiary nitrate appeared to decrease in the 2,4 HPN, this was not substantiated in the 2,4 HN. Thus, we were unable to reliably determine  $k_f$  and therefore only provide a lower bound.

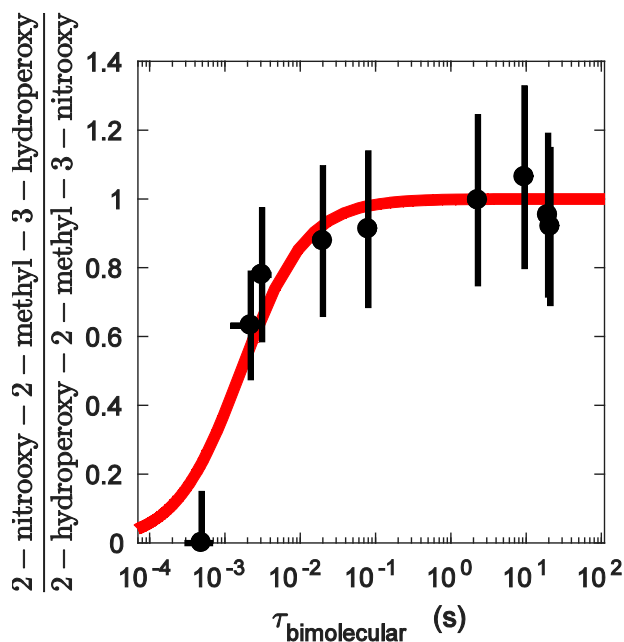


Figure S6. Experimental data used to constrain the rapid 1,6 RO<sub>2</sub> H-shift of the hydroperoxy hydrogens (ROO-H) in the 2,3 RO<sub>2</sub> at 296 K. The best fit (red line) is shown and is used to determine the experimental forward rate coefficient displayed in Scheme 2.

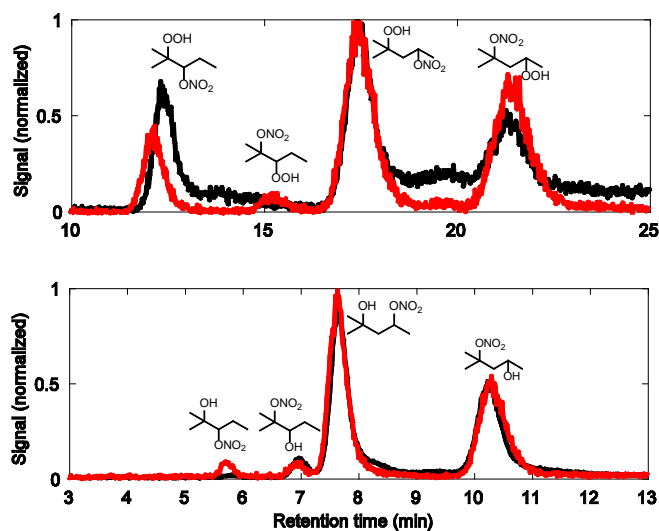


Figure S7. Chromatograms following oxidation of the substrate at  $\tau_{bimolecular} \sim 5 \times 10^{-5}$  s (black) and  $\tau_{bimolecular} \sim 2 \times 10^{-2}$  s (red). Shown are the HPN (top) and HN (bottom). The 2,3 RO<sub>2</sub> fail to achieve equilibrium at  $\tau_{bimolecular} \sim 5 \times 10^{-5}$  s, as demonstrated by the loss of the second HPN peak and the first HN peak. Retention times and peak shapes differ presumably due to slight differences in the instrumental configuration (the very short lifetime experiment was performed several months after the initial experiments). The signal has been normalized to the



intensity of the tallest peak.

## Computational

Multiconformer Transition State Theory (MC-TST) is used to calculate the rate coefficients in this work.<sup>12-15</sup> The reader is referred to the main article for an overview of the method.

### Tunneling

The 1D Eckart tunneling correction is used in our calculations.<sup>16</sup> The Eckart correction uses the imaginary frequency of the TS and the forward and reverse barrier height as input. An intrinsic reaction coordinate (IRC) is calculated from the B3LYP/6-31+G(d) TS conformer corresponding to the conformer lowest in zero-point corrected energy after optimization at the  $\omega$ B97X-D/aug-cc-pVTZ level of theory. The endpoints of the IRC are optimized at the B3LYP/6-31+G(d) level of theory and reoptimized with  $\omega$ B97X-D/aug-cc-pVTZ. Then, a ROHF-ROCCSD(T)-F12a/VDZ-F12// $\omega$ B97X-D/aug-cc-pVTZ single-point energy is calculated. The barrier heights use the single point energy and the  $\omega$ B97X-D/aug-cc-pVTZ zero-point correction, and the imaginary frequency is calculated with the  $\omega$ B97X-D functional and the aug-cc-pVTZ basis set.

## OH-Initiated Oxidation of 2-hydroperoxy-2-methylpentane

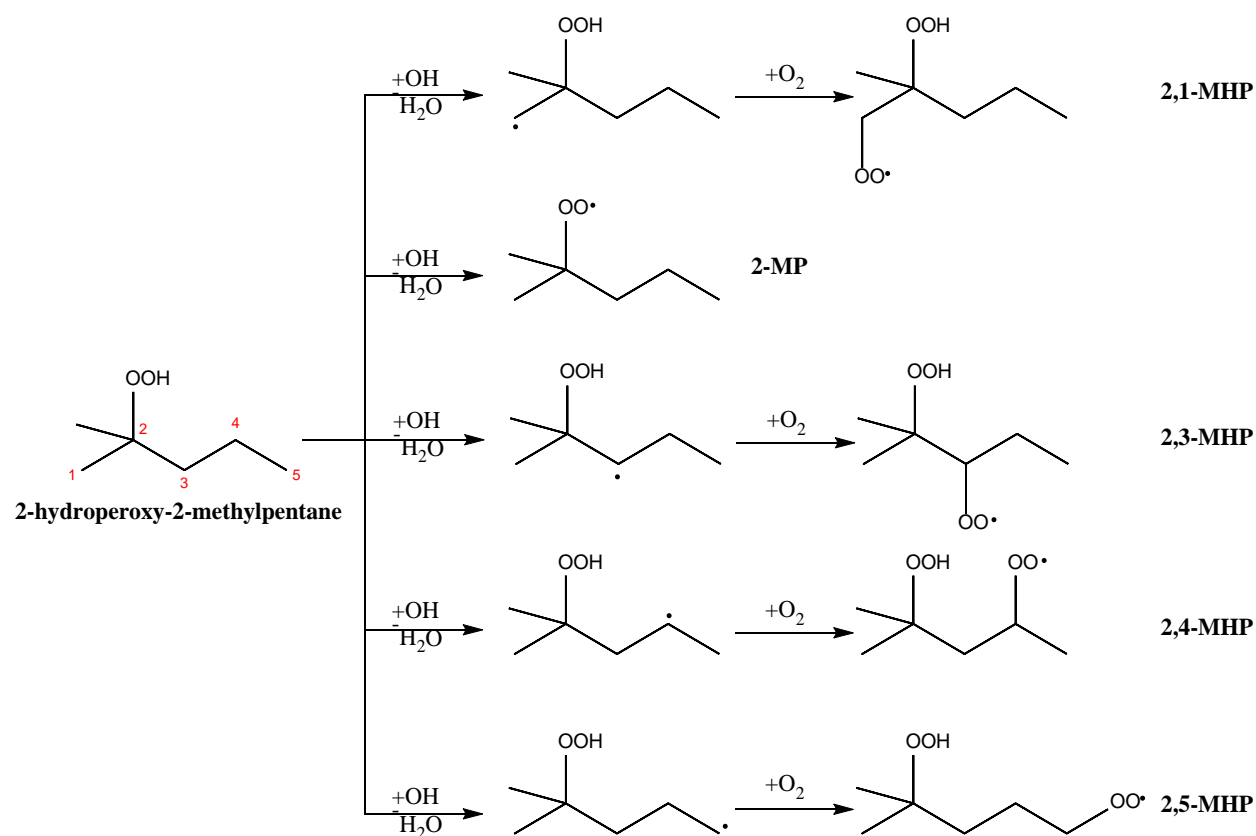


Figure S8. The  $RO_2$  formed following OH-initiated oxidation of 2-hydroperoxy-2-methylpentane. The atom numbering used for naming the compounds is shown in red on 2-hydroperoxy-2-methylpentane.

The reaction of 2-hydroperoxy-2-methylpentane with OH gives rise to multiple alkyl radicals (see Figure S). OH abstraction at the primary centers (C1 and C5) is expected to account for only a minor fraction of the total reactivity.<sup>17</sup> Abstraction at C3 and C4 leads to two  $RO_2$  that we refer to as 2,3-MHP and 2,4-MHP. Under this naming convention, the first number is the position of the hydroperoxy group and the second is the position of the  $RO_2$ . Abstraction of the hydrogen atom in the hydroperoxy group leads to a monofunctional  $RO_2$ , which we refer to as 2-MP. We consider the possibility that the alkyl radicals undergo H-shift chemistry prior to  $O_2$  addition. The alkyl radical preceding 2,4 MHP formation is investigated in order to rule out a fast

H-shift proceeding by abstraction of the hydroperoxide hydrogen (ROO-H). At 298.15 K, the rate coefficient is calculated to be  $2.1 \cdot 10^5 \text{ s}^{-1}$  and, therefore, this reaction is not expected to compete with  $\text{O}_2$  addition ( $\sim 10^7 \text{ s}^{-1}$ ) under the conditions of these experiments (1 atm in air). We assume that the same is true of the other alkyl radicals.

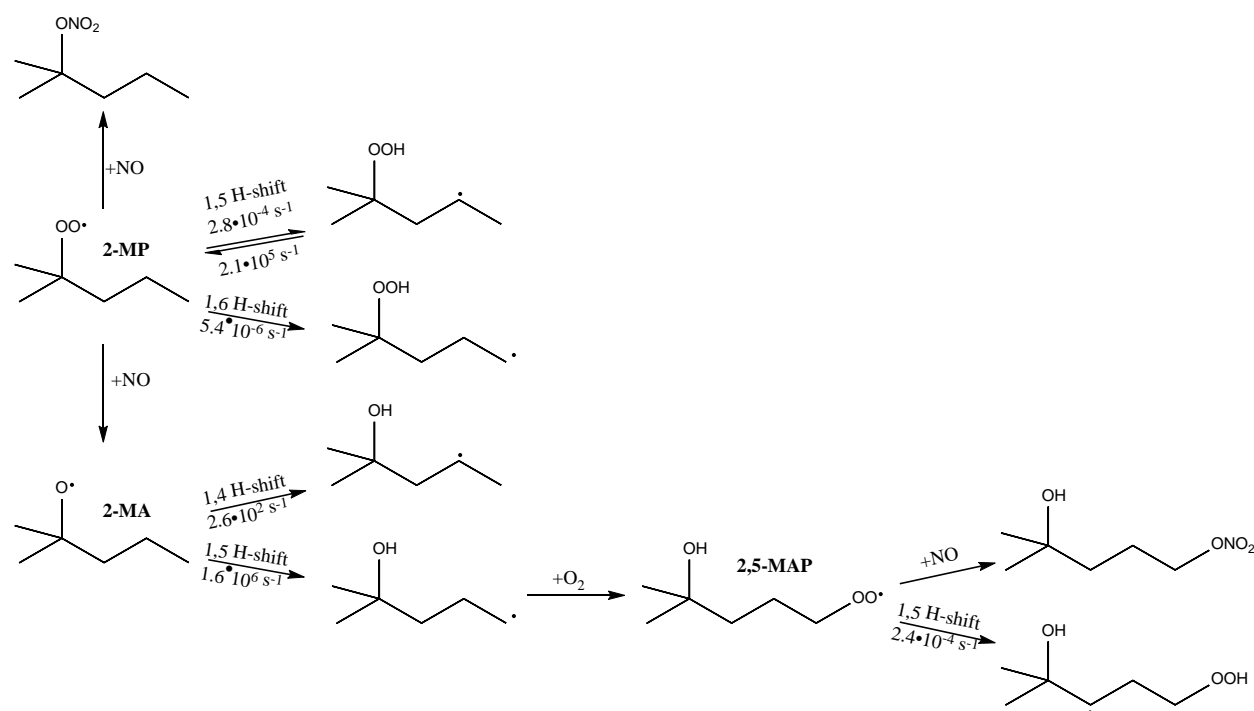


Figure S9. Reactions of 2-MP. Based on the reverse rate coefficient of the 2-MP 1,5 H-shift,  $\text{O}_2$  addition to the alkyl radical is expected to dominate. The rate coefficients shown are calculated at 298.15 K.

Selected reactions of 2-MP and its products are shown in Figure S9. 2-MP can undergo a 1,5 or 1,6 H-shift. These H-shifts are competing with reaction with NO to form either an organic nitrate or an alkoxy radical. The fastest H-shift of 2-MP is the 1,5 H-shift which has a rate coefficient of  $2.8 \cdot 10^{-4} \text{ s}^{-1}$ . Because of the slow H-shift rate coefficients, it is likely that 2-MP will react with NO to form an alkoxy radical, 2-MA, or an organic nitrate. We have calculated the rate

coefficients of both the 1,4 and 1,5 H-shifts arising from 2-MA. The 1,5 H-shift is the fastest with a rate coefficient of  $1.6 \cdot 10^6 \text{ s}^{-1}$ . This reaction leads to an alkyl radical, which can add  $\text{O}_2$  to form a new peroxy radical, 2,5-MAP. The fastest H-shift of 2,5-MAP is likely the 1,5 H-shift, which we calculate to have a rate coefficient of  $2.4 \cdot 10^{-4} \text{ s}^{-1}$ . Thus, bimolecular reaction is expected to dominate under our experimental conditions.

The possible 1,4 H-shift of 2,3-MHP abstracting from the C4 position is expected to be slow based on the calculated rate coefficients of the 1,4 H-shift in 3,2-MHP and those calculated by Otkjær et al.,<sup>18</sup> as are the H-shifts that abstract from the methyl groups. 2,3-MHP can react by a 1,6-OOH H-shift to form 3,2-MHP. The 1,6-OOH has an equilibrium constant of 0.60 at 298.15 K. Although lower in abundance than 2,3-MHP, 3,2-MHP can undergo a 1,4 H-shift abstracting at C3 or a 1,5 H-shift abstracting at C4. The 1,4 H-shift is expected to be faster than other 1,4 H-shifts due to the OOH group at C3, but we also investigated the 1,5 H-shift because 1,5 H-shifts generally are among the fastest peroxy radical H-shifts.<sup>19-20</sup> We calculate both H-shifts to be relatively slow, with the fastest forward rate coefficient being  $5.3 \cdot 10^{-4} \text{ s}^{-1}$  for the 1,5 H-shift. Again, we expect bimolecular reaction to dominate under the experimental conditions.

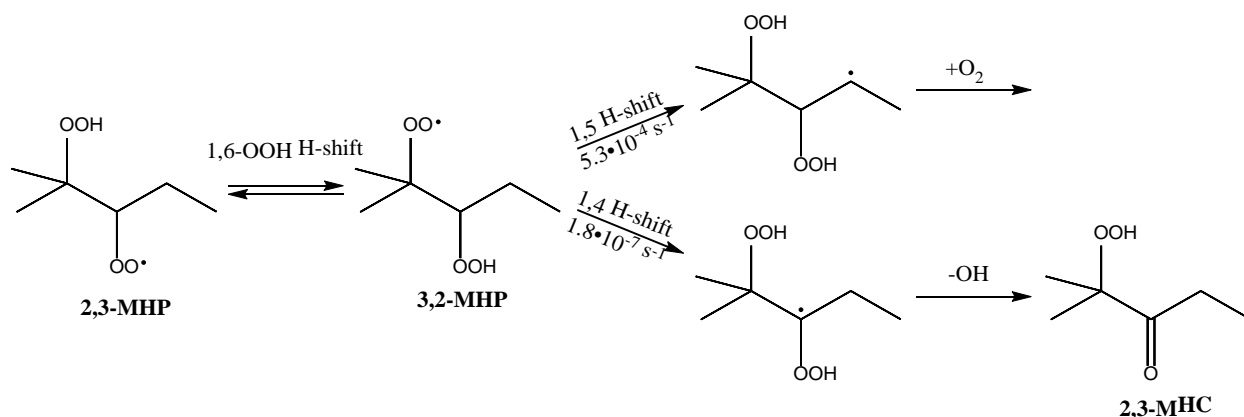


Figure S10. H-shift reactions of 2,3-MHP. Reactions with NO or  $\text{HO}_2$  are omitted for clarity. The

rate coefficients shown are calculated at 298.15 K.

The rapid scrambling between the 2,4- and 4,2-MHP has an equilibrium constant of 3.1 in favor of the 4,2-MHP. The scrambling leads to the 1,5  $\alpha$ -OOH H-shift which has a relatively large forward rate coefficient of  $0.054\text{ s}^{-1}$  (298.15 K). The reverse reaction was not calculated as the product is expected to decompose promptly, forming a carbonyl and releasing OH. We expect the 2,4 methyl-hydroperoxy-carbonyl (2,4 MHC) to be a major product of 2,4-MHP, with the yield depending on  $\tau_{\text{bimolecular}}$ .

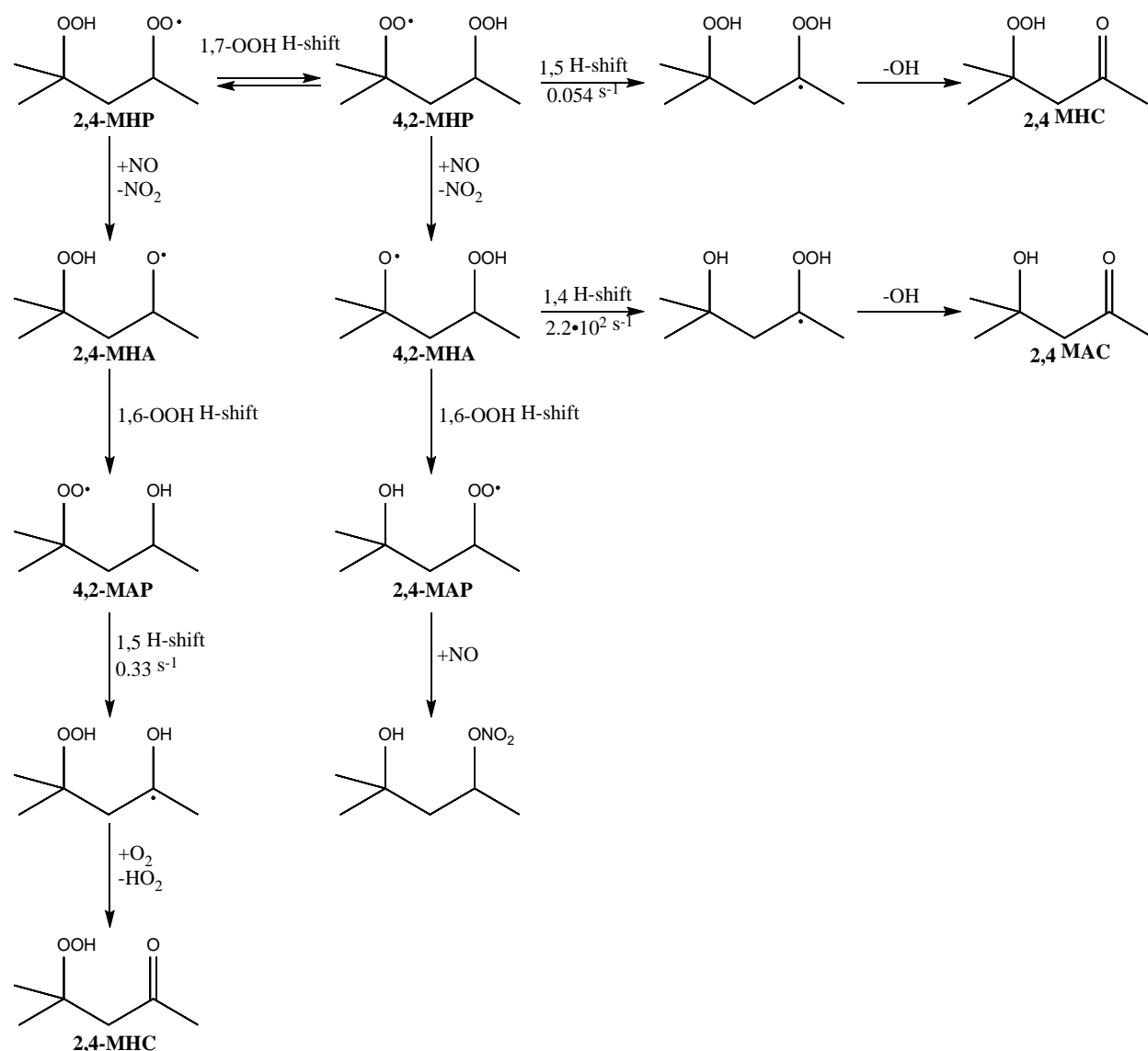


Figure S11. H-shift reactions of 2,4-MHP. Only selected reactions with NO or HO<sub>2</sub> are shown for clarity. The rate coefficients shown are calculated at 298.15 K.

At high NO concentrations, both 2,4-MHP and 4,2-MHP can react with NO to form alkoxy radicals, 2,4-MHA and 4,2-MHA, respectively. Both alkoxy radicals undergo a 1,6-OOH H-shift, expected to be very fast. For 2,4-MHA, this leads to the peroxy radical 4,2-MAP. 4,2-MAP undergoes a 1,5 H-shift with a rate coefficient of  $0.33 \text{ s}^{-1}$ , leading to the formation of a carbonyl (2,4-MHC) through reaction with O<sub>2</sub>. This is the same carbonyl as the one formed by the 1,5 H-shift of the 4,2-MHP. The other alkoxy radical, 4,2-MHA, undergoes either a 1,4 H-shift to

produce a carbonyl, or a 1,6-OOH H-shift. The 1,4 H-shift has a rate coefficient of  $2.2 \cdot 10^2 \text{ s}^{-1}$ . We expect 4,2-MHA to react via the 1,6-OOH H-shift to form 2,4-MAP, which likely has no fast intramolecular chemistry.

### OH-Initiated Oxidation of 2-hydroperoxypentane

As a theoretical complement to the 2-hydroperoxy-2-methylpentane calculations, we studied some of the reactions following OH-initiated oxidation of 2-hydroperoxypentane (see Figure S12).

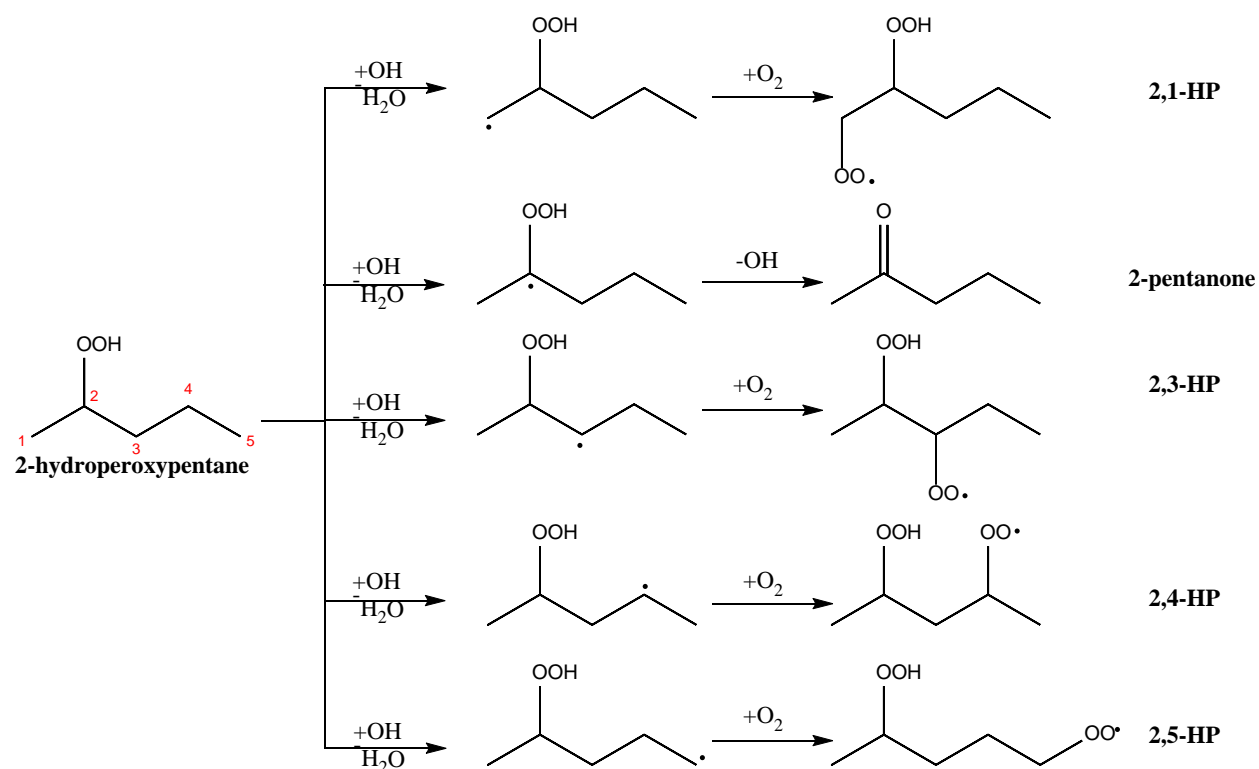


Figure S12. The RO<sub>2</sub> formed following OH-initiated oxidation of 2-hydroperoxypentane. The atom numbering used to name the peroxy radicals is shown in red on 2-hydroperoxypentane.

Abstraction by OH at C2, which yields 2-pentanone, is likely the major reaction but is not of interest here. The most important peroxy radicals in our study are the 2,3- and 2,4-HP, as abstraction at C1 and C5 is expected to be minor. The abstraction of the ROO-H likely comprises

a significant part of the branching ratio, but the reactions of the resulting peroxy radical are not studied here. Since both 2,3-HP and 2,4-HP have two chiral centers, a total of four diastereomers are produced. We have studied the S,R and S,S diastereomers. The enantiomers are expected to have identical reactivities. The possible H-shift reactions of 2,3-HP are shown in Figure S13.

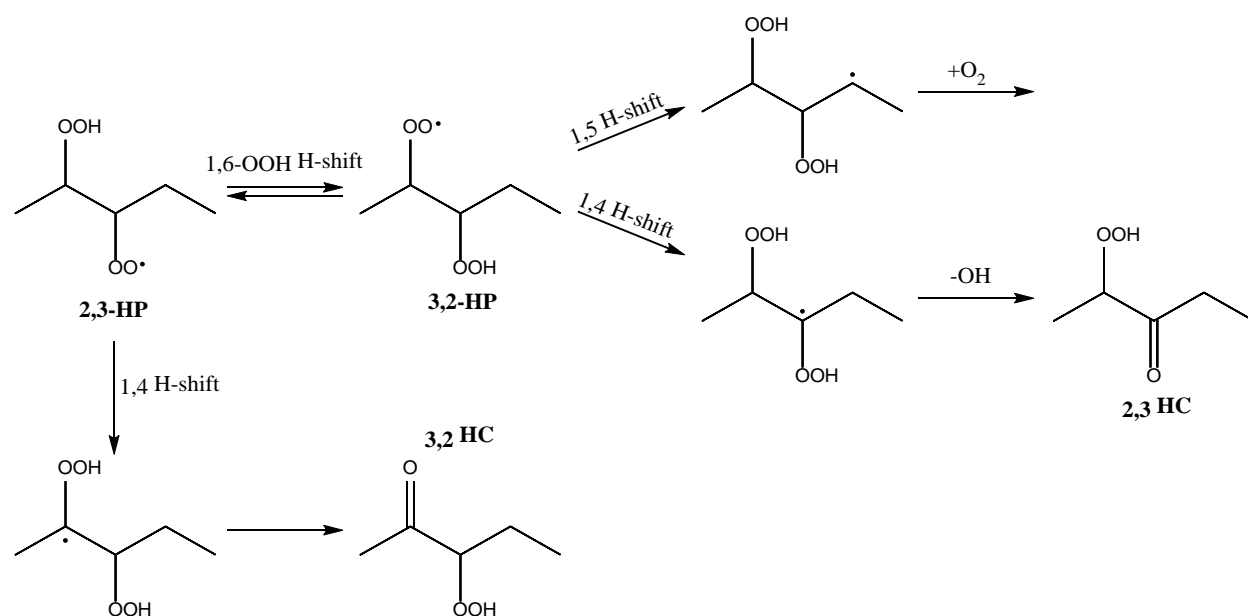


Figure S13. H-shift reactions of 2,3-HP. Reactions with NO or HO<sub>2</sub> are omitted for brevity.

The possible 1,4 H-shift of 2,3-HP is slow for both diastereomers, with the largest rate coefficient of  $9.0 \times 10^{-6} \text{ s}^{-1}$  for the S,S diastereomer. 2,3-HP can also undergo a rapid 1,6-OOH H-shift to form 3,2-HP. The 1,6-OOH H-shift of 2,3-HP has an equilibrium constant of 1.4 in favor of 3,2-HP for both diastereomers. 3,2-HP can undergo either a 1,4 or 1,5 H-shift. Both are slow with the largest rate coefficient being the 1,5 H-shift of (S,R) 3,2-HP with a rate coefficient of  $6.1 \times 10^{-4} \text{ s}^{-1}$ . We expect bimolecular reaction to dominate even with relatively low NO concentrations. The rate coefficients of 2,3-HP and 3,2-HP are shown in Table S3.



Table S3. Calculated rate coefficients in the oxidation of 2-hydroperoxypentane at 298.15 K.

Reactant	H-shift	Isomer	$k_f$ (s <sup>-1</sup> )	$k_r$ (s <sup>-1</sup> )
2,3-HP	1,4	S,R	$5.0 \times 10^{-6}$	-
		S,S	$9.0 \times 10^{-6}$	-
3,2-HP	1,4	S,R	$8.8 \times 10^{-7}$	-
		S,S	$4.8 \times 10^{-6}$	-
	1,5	S,R	$6.1 \times 10^{-4}$	$2.0 \times 10^5$
		S,S	$2.4 \times 10^{-4}$	$5.4 \times 10^4$
2,4-HP	1,5	S,R	0.046	-
		S,S	0.12	-

In Figure S14 we show the H-shift reactions of 2,4 HP leading to the formation of a ketone. The rate coefficients of the 1,5 H-shift are shown in Table S.

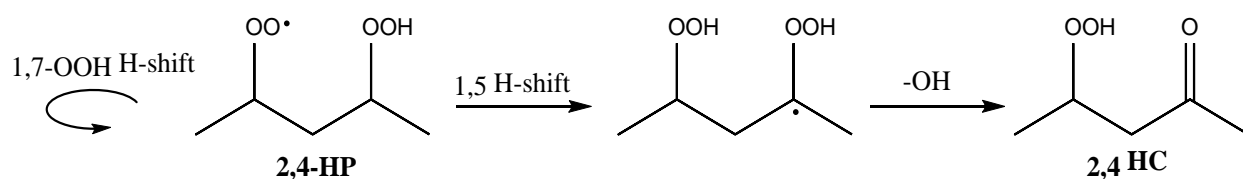


Figure S14. The reactions of 2,4-HP. The curved arrow represents the 1,7-OOH H-shift which, because of symmetry, forms a diastereomer of the same compound. Reactions with NO and HO<sub>2</sub>

are omitted for brevity.

### Temperature Dependencies

The temperature dependencies shown here are obtained by calculating the MC-TST rate coefficients every 5 K between 290-320 K. The MC-TST rate coefficients without tunneling are plotted against  $1/T$ , while the tunneling corrections are plotted against  $1/T^3$ . Exponential functions are used to fit the data points. The prefactors of the two exponentials are multiplied to give the factor listed in Table S4. The rate coefficients calculated at 320 K warrant a higher value for the cutoff after B3LYP optimizations to keep the cutoff at a constant value of  $k_B T$ , but the error induced by this is likely negligible in the temperature range studied. The expressions in Table S4 and Table S5 yield rate coefficients within 2% of the calculated MC-TST values.

Table S4. Temperature dependencies of the H-shift rate coefficients in the OH oxidation of 2-hydroperoxy-2-methylpentane. They are intended for use in the range 290-320 K.

Reactant	H-shift	Direction	$k \text{ (s}^{-1}\text{)}$
2-MP	1,5	Forward	$1.4274 \times 10^{12} \times \exp\left(\frac{-11628}{T}\right) \times \exp\left(\frac{7.5299 \times 10^7}{T^3}\right)$
		Reverse	$2.6380 \times 10^{15} \times \exp\left(\frac{-7783.8}{T}\right) \times \exp\left(\frac{7.5299 \times 10^7}{T^3}\right)$
	1,6	Forward	$4.4977 \times 10^{11} \times \exp\left(\frac{-12528}{T}\right) \times \exp\left(\frac{8.1210 \times 10^7}{T^3}\right)$
2-MA	1,4	Forward	$9.4683 \times 10^{11} \times \exp\left(\frac{-7986.6}{T}\right) \times \exp\left(\frac{1.2625 \times 10^8}{T^3}\right)$
	1,5	Forward	$2.9427 \times 10^{11} \times \exp\left(\frac{-4345.7}{T}\right) \times \exp\left(\frac{6.4884 \times 10^7}{T^3}\right)$
2,5-MAP	1,5	Forward	$1.4036 \times 10^{11} \times \exp\left(\frac{-10869}{T}\right) \times \exp\left(\frac{6.5382 \times 10^7}{T^3}\right)$
3,2-MHP	1,4	Forward	$1.0845 \times 10^{12} \times \exp\left(\frac{-14830}{T}\right) \times \exp\left(\frac{1.7223 \times 10^8}{T^3}\right)$

	1,5	Forward	$6.6275 \times 10^{12} \times \exp\left(\frac{-11947}{T}\right) \times \exp\left(\frac{7.9513 \times 10^7}{T^3}\right)$
		Reverse	$6.3796 \times 10^{12} \times \exp\left(\frac{-6173.0}{T}\right) \times \exp\left(\frac{7.9513 \times 10^7}{T^3}\right)$
4,2-MHP	1,5	Forward	$1.6828 \times 10^{12} \times \exp\left(\frac{-10272}{T}\right) \times \exp\left(\frac{8.9426 \times 10^7}{T^3}\right)$
4,2-MHA	1,4	Forward	$4.6678 \times 10^{13} \times \exp\left(\frac{-8320.6}{T}\right) \times \exp\left(\frac{4.8739 \times 10^7}{T^3}\right)$
4,2-MAP	1,5	Forward	$9.5219 \times 10^{11} \times \exp\left(\frac{-9543.6}{T}\right) \times \exp\left(\frac{8.8195 \times 10^7}{T^3}\right)$

Table S5. Temperature dependencies of the H-shift rate coefficients in the OH oxidation of 2-hydroperoxypentane. They are intended for use in the range 290-320 K.

Reactant	H-shift	Isomer	Direction	$k \text{ (s}^{-1}\text{)}$
2,3-HP	1,4	S,R	Forward	$7.6094 \times 10^{12} \times \exp\left(\frac{-14546}{T}\right) \times \exp\left(\frac{1.8308 \times 10^8}{T^3}\right)$
		S,S	Forward	$6.1015 \times 10^{12} \times \exp\left(\frac{-14303}{T}\right) \times \exp\left(\frac{1.8310 \times 10^8}{T^3}\right)$
3,2-HP	1,4	S,R	Forward	$1.1101 \times 10^{12} \times \exp\left(\frac{-14472}{T}\right) \times \exp\left(\frac{1.8180 \times 10^8}{T^3}\right)$
		S,S	Forward	$3.9137 \times 10^{12} \times \exp\left(\frac{-14399}{T}\right) \times \exp\left(\frac{1.8655 \times 10^8}{T^3}\right)$
	1,5	S,R	Forward	$5.9170 \times 10^{12} \times \exp\left(\frac{-11913}{T}\right) \times \exp\left(\frac{8.3448 \times 10^7}{T^3}\right)$
			Reverse	$3.0588 \times 10^{12} \times \exp\left(\frac{-5868.6}{T}\right) \times \exp\left(\frac{8.3448 \times 10^7}{T^3}\right)$
		S,S	Forward	$4.8330 \times 10^{12} \times \exp\left(\frac{-12180}{T}\right) \times \exp\left(\frac{8.7302 \times 10^7}{T^3}\right)$

			Reverse	$4.1323 \times 10^{11} \times \exp\left(\frac{-5707.4}{T}\right) \times \exp\left(\frac{8.7302 \times 10^7}{T^3}\right)$
2,4-HP	1,5	S,R	Forward	$1.8270 \times 10^{11} \times \exp\left(\frac{-9818.4}{T}\right) \times \exp\left(\frac{1.0411 \times 10^8}{T^3}\right)$
		S,S	Forward	$4.3365 \times 10^{11} \times \exp\left(\frac{-9701.6}{T}\right) \times \exp\left(\frac{9.5707 \times 10^7}{T^3}\right)$

Values used in the MC-TST equation at 298.15 K

Table S6. Values of the components of the MC-TST equation used to calculate the rate coefficients in the oxidation of 2-hydroperoxy-2-methylpentane at 298.15 K.

Reactant	Reaction	$\kappa$	$Q_R$	$Q_{TS}$	$Q_P$	$E_f$ (kcal/mol)	$E_r$ (kcal/mol)
2-MP	1,5 H-shift	$4.63 \times 10^1$	$6.83 \times 10^8$	$5.79\text{E} \times 10^7$	$2.6 \times 10^9$	23.1	10.2
	1,6 H-shift	$6.60 \times 10^1$	$6.83 \times 10^8$	$2.58\text{E} \times 10^7$	-	25.2	-
2-MA	1,4 H-shift	$1.52 \times 10^2$	$1.73 \times 10^8$	$1.56\text{E} \times 10^7$	-	15.7	-
	1,5 H-shift	$2.34 \times 10^1$	$1.73 \times 10^8$	$6.93\text{E} \times 10^6$	-	8.95	-
2,5-MAP	1,5 H-shift	$3.07 \times 10^1$	$2.58 \times 10^{10}$	$3.58\text{E} \times 10^8$	-	21.9	-
3,2-MHP	1,4 H-shift	$4.67 \times 10^2$	$1.07 \times 10^{10}$	$1.53 \times 10^9$	-	29.1	-
	1,5 H-shift	$5.62 \times 10^1$	$1.07 \times 10^{10}$	$3.49 \times 10^9$	$6.72\text{E} \times 10^9$	23.6	12.5
4,2-MHP	1,5 H-shift	$6.70 \times 10^1$	$1.34 \times 10^{10}$	$2.36 \times 10^9$	-	20.6	-
4,2-MHA	1,4 H-shift	8.30	$2.47\text{E} \times 10^8$	$4.54\text{E} \times 10^8$	-	15.9	-

4,2-MAP	1,5 H-shift	$5.40 \times 10^1$	$4.61 \text{E} \times 10^9$	$3.69 \text{E} \times 10^8$	-	19.0	-
---------	-------------	--------------------	-----------------------------	-----------------------------	---	------	---

Table S7. Values of the components of the MC-TST equation used to calculate the rate coefficients in the oxidation of 2-hydroperoxypentane at 298.15 K.

Reactant	H-shift	Isomer	$\kappa$	$Q_R$	$Q_{TS}$	$Q_P$	$E_f$ kcal/mol	$E_r$ kcal/mol
2,3-HP	1,4	S,R	$1.52 \times 10^3$	$7.48 \times 10^8$	$5.08 \times 10^8$	-	28.8	-
		S,S	$1.52 \times 10^3$	$1.67 \times 10^9$	$8.92 \times 10^8$	-	28.3	-
3,2-HP	1,4	S,R	$6.97 \times 10^2$	$2.56 \times 10^9$	$1.34 \times 10^9$	-	29.2	-
		S,S	$1.65 \times 10^3$	$1.42 \times 10^9$	$5.62 \times 10^8$	-	28.6	-
	1,5	S,R	$6.18 \times 10^1$	$2.33 \times 10^9$	$1.76 \times 10^9$	$4.02 \times 10^9$	24.1	12.2
		S,S	$6.54 \times 10^1$	$1.42 \times 10^9$	$3.24 \times 10^8$	$1.02 \times 10^{10}$	24.0	11.4
2,4-HP	1,5	S,R	$8.13 \times 10^1$	$1.24 \times 10^{10}$	$5.99 \times 10^8$	-	20.1	-
		S,S	$7.76 \times 10^1$	$7.62 \times 10^9$	$5.39 \times 10^8$	-	19.7	-

## Values used for the Eckart Tunneling Correction

Table S8. Components used as input for the calculation of the Eckart tunneling correction in the rate coefficients of the oxidation of 2-hydroperoxy-2-methylpentane.

Reactant	H-Shift	E <sub>f</sub> (kcal/mol)	E <sub>r</sub> (kcal/mol)	Imag. Freq. $\nu$ ( $cm^{-1}$ )
2-MP	1,5	21.8	8.22	1858
	1,6	23.9	8.40	1950
2-MA	1,4	15.7	24.4	1793
	1,5	8.62	14.4	1647
2,5-MAP	1,5	21.1	7.30	1803
3,2-MHP	1,4	26.4	22.6	1818
	1,5	20.8	8.53	1890
4,2-MHP	1,5	18.8	10.2	1834
4,2-MHA	1,4	11.9	27.8	1297
4,2-MAP	1,5	17.8	11.0	1756

Table S9. Components used as input for the calculation of the Eckart tunneling correction in the rate coefficients of the oxidation of 2-hydroperoxypentane.

Reactant	H-Shift	Isomer	E <sub>f</sub> (kcal/mol)	E <sub>r</sub> (kcal/mol)	Imag. Freq. $\nu$ ( $cm^{-1}$ )
2,3-HP	1,4 H-shift	S,R	26.6	19.0	2027
		S,S	26.6	19.0	2027
3,2-HP	1,4 H-shift	S,R	28.3	22.2	1858
		S,S	27.9	19.3	2023
	1,5 H-shift	S,R	20.7	9.1	1877
		S,S	20.8	9.8	1850

2,4-HP	1,5 H-shift	S,R	19.5	13.4	1761
		S,S	19.8	11.1	1824

#### Rate Constants at the $\omega$ B97X-D/aug-cc-pVTZ level of theory at 298.15 K

In addition to the rate constants presented in the main manuscript and above (which are calculated using ROHF-ROCCSD(T)-F12a/VDZ-F12// $\omega$ B97X-D/aug-cc-pVTZ), we here report the rate constants calculated using  $\omega$ B97X-D/aug-cc-pVTZ.

Table S11. Rate constants in the oxidation of 2-hydroperoxy-2-methylpentane calculated at the  $\omega$ B97X-D/aug-cc-pVTZ level of theory at 298.15 K.

Reactant	H-Shift	$k_f$ (s <sup>-1</sup> )	$k_r$ (s <sup>-1</sup> )
2-MP	1,5	$7.5 \times 10^{-5}$	$4.6 \times 10^6$
	1,6	$7.0 \times 10^{-7}$	-
2-MA	1,4	$4.9 \times 10^2$	-
	1,5	$2.2 \times 10^6$	-
2,5-MAP	1,5	$4.7 \times 10^{-5}$	-
2,3-MHP	1,6-OOH	$4.0 \times 10^3$	$4.9 \times 10^3$
3,2-MHP	1,4	$2.8 \times 10^{-7}$	-
	1,5	$8.8 \times 10^{-5}$	$2.8 \times 10^6$
2,4-MHP	1,7-OOH	$1.2 \times 10^6$	$6.0 \times 10^5$
4,2-MHP	1,5	$3.7 \times 10^{-2}$	-
2,4-MHA	1,6-OOH	$7.8 \times 10^9$	-
4,2-MHA	1,4	$6.3 \times 10^3$	
4,2-MHA	1,6-OOH	$1.8 \times 10^{10}$	
4,2-MAP	1,5	$1.3 \times 10^{-1}$	$1.5 \times 10^5$

Table S12. Rate constants for reactions in the oxidation of 2-hydroperoxy-pentane calculated at the  $\omega$ B97X-D/aug-cc-pVTZ level of theory at 298.15 K.

Reactant	H-shift	Isomer	$k_f$ (s <sup>-1</sup> )	$k_r$ (s <sup>-1</sup> )
2,3-HP	1,4	S,R	$5.0 \times 10^{-6}$	-
		S,S	$9.8 \times 10^{-6}$	-
	1,6-OOH	S,R	$8.1 \times 10^2$	$6.4 \times 10^2$
		S,S	$3.5 \times 10^3$	$2.8 \times 10^3$
3,2-HP	1,4	S,R	$8.2 \times 10^{-7}$	-
		S,S	$3.7 \times 10^{-6}$	-
	1,5	S,R	$2.1 \times 10^{-4}$	$7.1 \times 10^6$
		S,S	$7.3 \times 10^{-5}$	$1.5 \times 10^{-6}$
2,4-HP	1,5	S,R	$3.8 \times 10^{-2}$	-
		S,S	$4.6 \times 10^{-2}$	-
	1,7-OOH	S,R	$8.7 \times 10^4$	$8.7 \times 10^{-4}$
		S,S	$7.1 \times 10^{-4}$	$7.1 \times 10^{-4}$



## References

1. Teng, A. P.; Crounse, J. D.; Wennberg, P. O., Isoprene Peroxy Radical Dynamics. *J. Am. Chem. Soc.* **2017**, *139* (15), 5367-5377.
2. Praske, E.; Otkjær, R. V.; Crounse, J. D.; Hethcox, J. C.; Stoltz, B. M.; Kjaergaard, H. G.; Wennberg, P. O., Atmospheric Autoxidation Is Increasingly Important in Urban and Suburban North America. *Proc. Natl. Acad. Sci. U.S.A.* **2018**, *115* (1), 64-69.
3. Crounse, J. D.; Paulot, F.; Kjaergaard, H. G.; Wennberg, P. O., Peroxy Radical Isomerization in the Oxidation of Isoprene. *Phys. Chem. Chem. Phys.* **2011**, *13* (30), 13607-13613.
4. Atkinson, R.; Baulch, D. L.; Cox, R. A.; Crowley, J. N.; Hampson, R. F.; Hynes, R. G.; Jenkin, M. E.; Rossi, M. J.; Troe, J., Evaluated Kinetic and Photochemical Data for Atmospheric Chemistry: Volume I - Gas Phase Reactions of O<sub>x</sub>, HO<sub>x</sub>, NO<sub>x</sub> and SO<sub>x</sub> Species. *Atmos. Chem. Phys.* **2004**, *4*, 1461-1738.
5. Wennberg, P. O.; Bates, K. H.; Crounse, J. D.; Dodson, L. G.; McVay, R. C.; Mertens, L. A.; Nguyen, T. B.; Praske, E.; Schwantes, R. H.; Smarte, M. D., et al., Gas-Phase Reactions of Isoprene and Its Major Oxidation Products. *Chem. Rev.* **2018**, *118* (7), 3337-3390.
6. Teng, A. P.; Crounse, J. D.; Lee, L.; St. Clair, J. M.; Cohen, R. C.; Wennberg, P. O., Hydroxy Nitrate Production in the Oh-Initiated Oxidation of Alkenes. *Atmos. Chem. Phys.* **2015**, *15* (8), 4297-4316.
7. Atkinson, R.; Carter, W. P. L.; Winer, A. M., Effects of Temperature and Pressure on Alkyl Nitrate Yields in the NO<sub>x</sub> Photooxidations of Normal-Pentane and Normal-Heptane. *J. Phys. Chem.* **1983**, *87* (11), 2012-2018.
8. Garden, A. L.; Paulot, F.; Crounse, J. D.; Maxwell-Cameron, I. J.; Wennberg, P. O.; Kjaergaard, H. G., Calculation of Conformationally Weighted Dipole Moments Useful in Ion-Molecule Collision Rate Estimates. *Chem. Phys. Lett.* **2009**, *474* (1-3), 45-50.
9. Su, T.; Chesnavich, W. J., Parametrization of the Ion-Polar Molecule Collision Rate-Constant by Trajectory Calculations. *J. Chem. Phys.* **1982**, *76* (10), 5183-5185.
10. O'Haver, T. Interactive Peak Fitter. Available at <https://terpconnect.umd.edu/~toh/spectrum/Interactivepeakfitter.Htm>. Accessed January 8, 2017.
11. Saunders, S. M.; Jenkin, M. E.; Derwent, R. G.; Pilling, M. J., Protocol for the Development of the Master Chemical Mechanism, MCM V3 (Part a): Tropospheric Degradation of Non-Aromatic Volatile Organic Compounds. *Atmos. Chem. Phys.* **2003**, *3*, 161-180.
12. Eyring, H., The Activated Complex and the Absolute Rate of Chemical Reactions. *Chemical Reviews* **1935**, *17* (1), 65-77.
13. Evans, M. G.; Polanyi, M., Some Applications of the Transition State Method to the Calculation of Reaction Velocities, Especially in Solution. *Trans. Faraday Soc.* **1935**, *31* (0), 875-894.
14. Vereecken, L.; Peeters, J., The 1,5-H-Shift in 1-Butoxy: A Case Study in the Rigorous Implementation of Transition State Theory for a Multirotamer System. *J. Chem. Phys.* **2003**, *119* (10), 5159-5170.
15. Møller, K. H.; Otkjær, R. V.; Hyttinen, N.; Kurtén, T.; Kjaergaard, H. G., Cost-Effective Implementation of Multiconformer Transition State Theory for Peroxy Radical Hydrogen Shift Reactions. *J. Phys. Chem. A* **2016**, *120* (51), 10072-10087.
16. Eckart, C., The Penetration of a Potential Barrier by Electrons. *Physical Review* **1930**, *35* (11), 1303-1309.

17. Kwok, E. S. C.; Atkinson, R., Estimation of Hydroxyl Radical Reaction Rate Constants for Gas-Phase Organic Compounds Using a Structure-Reactivity Relationship: An Update. *Atmos. Environ.* **1995**, 29 (14), 1685-1695.
18. Otkjær, R. V.; Jakobsen, H. H.; Tram, C. M.; Kjaergaard, H. G., Calculated Hydrogen Shift Rate Constants in Substituted Alkyl Peroxy Radicals. *J. Phys. Chem. A* **2018**.
19. Jørgensen, S.; Knap, H. C.; Otkjær, R. V.; Jensen, A. M.; Kjeldsen, M. L. H.; Wennberg, P. O.; Kjaergaard, H. G., Rapid Hydrogen Shift Scrambling in Hydroperoxy-Substituted Organic Peroxy Radicals. *J. Phys. Chem. A* **2016**, 120 (2), 266-275.
20. Crounse, J. D.; Nielsen, L. B.; Jørgensen, S.; Kjaergaard, H. G.; Wennberg, P. O., Autoxidation of Organic Compounds in the Atmosphere. *J. Phys. Chem. Lett.* **2013**, 4 (20), 3513-3520.